Available online at www.sciencedirect.com
SCIENCE DIRECT®
Thin Solid Films 443 (2003) 97–107
thin solid films
www.elsevier.com/locate/tsf

Chemical vapor deposition of tungsten silicide (WSi_x) for high aspect ratio applications

B. Sell[a,*], A. Sänger[a], G. Schulze-Icking[b], K. Pomplun[a], W. Krautschneider[c]

[a]*Infineon Technologies, Königsbrücker Strasse 180, 01099 Dresden, Germany*
[b]*Infineon Technologies AG, Balanstrasse 73, 81541 Munich, Germany*
[c]*TU Hamburg-Harburg, Techn. Electronics, Eissendorfer Strasse 38, 21071 Hamburg, Germany*

Received 15 January 2003; received in revised form 24 May 2003; accepted 13 June 2003

Abstract

Chemical vapor deposition of tungsten silicide into high aspect ratio trenches has been investigated using a commercial 8-inch Applied Materials *Centura* single wafer deposition tool. For an in-depth study of both step coverage and stoichiometry, a combined chemistry/topography simulator has been developed. Dichlorosilane reduction of tungsten hexafluoride (WF_6) has been identified as a suitable chemistry to fill deep trenches with tungsten disilicide, while for WF_6 reduction with silane (SiH_4) or disilane (Si_2H_6) fundamental drawbacks have been identified for extreme aspect ratios. In the process range under study, good agreement is observed between the simulated step coverages and those obtained from scanning electron microscope images. The simulations predict a deposition regime in which both good step coverage and a suitable stoichiometry are achieved inside deep trenches.

Keywords: Chemical vapor deposition; Deposition process; Nanostructures; Tungsten

1. Introduction

With continuously decreasing groundrules in modern ULSI manufacturing, there exists a strong demand for partially replacing doped polysilicon with metals or other low resistivity materials. Refractory metal silicides, for instance, are widely used as part of the gate stack in dynamic random access memory (DRAM) manufacturing. Another possible application for low resistivity materials is in the capacitor of deep trench-DRAM or in vias of stacked DRAM cells. Both products suffer from the fact that the serial resistance of the inner electrode (plug, deep trench-DRAM) or vias (stacked-DRAM) increases with the square of the inverse ground rule. This effect is further enhanced since the requirement of a constant capacitance of 25 fF leads to deeper trenches (or higher stacks, respectively) in future DRAMs. Thus, for shrinking the ground rule, the cross-section of the plugs (deep trench) or vias (stacked) decreases, while at the same time their length increases. To still maintain sufficient current into and out of DRAM capacitors, low resistivity plugs/vias are indispensable for future DRAM generations.

Refractory metal silicides exhibit properties that make them prime candidates for replacing doped polysilicon where low resistivity is required. Given the right stoichiometry, they are stable up to high temperatures, show good adhesion and also a good dry etchability [1]. Silicides can be prepared in two different ways. Pure metal can either be deposited on silicon and transformed into a silicide via thermal annealing or metal and silicon can be co-deposited, which immediately leads to a silicide layer. The latter process is generally preferred since it leads to lower mechanical stress and a smoother silicide–silicon interface [2].

In this paper, we discuss the chemical vapor deposition (CVD) of low resistivity tungsten silicide (WSi_x) into features with large aspect ratios. While we focus on deep trench plugs of trench DRAMs (as manufactured by Infineon Technologies), all results presented in

*Corresponding author. Tel.: +1-971-2148-783.
E-mail address: ben.sell@t-online.de (B. Sell).

0040-6090/03/$ - see front matter © 2003 Elsevier B.V. All rights reserved.
doi:10.1016/S0040-6090(03)00922-2

this paper also apply to vias of stacked DRAMs with only minor modifications.

Key requirements for a WSi_x-plug are thermal stability in contact with polysilicon up to frontend processing temperatures ($T \approx 1400$ K), good step coverage in trenches with aspect ratios $\geqslant 50{:}1$ and sufficiently uniform stoichiometry along the depth of the deep trench. The only thermodynamically stable phase in contact with silicon is WSi_2. While silicon-rich WSi_x-films ($x > 2.3$) exhibit smooth film-to-substrate interface [3], they are thermally unstable and segregate the excess silicon as silicon crystallites or increase the thickness of the underlying polysilicon [4]. Tungsten-rich films ($x < 2.0$), on the other hand, are also thermally unstable and lead to the consumption of the underlying polysilicon layer during anneal steps later in the process [5]. Thus, the composition of tungsten silicide layers in frontend processes should always be larger than 2 and ideally approximately 2.3 [6]. Note that slightly less stringent limitations apply to vias in stacked-DRAM since those are not subject to high temperature anneals.

In this paper, we demonstrate a procedure to choose appropriate precursors and process conditions for tungsten silicide CVD into structures with extreme aspect ratios. An optimized process with both good step coverage and suitable stoichiometry for frontend applications will be proposed.

This paper is organized as follows: Section 2 describes the general requirements on growth kinetics to achieve good step coverage in high AR structures. Selected precursors currently available for WSi_x-CVD are briefly discussed in Section 3 and evaluated in terms of the proposed application. Experimental results of the investigated deposition process are presented in Section 4 and compared to chemistry/topography simulations on the feature scale in Section 5. Experimental and simulation results are discussed in Section 6, followed by a summary and a conclusion in Section 7.

2. Growth kinetics

Generally, CVD can be divided into four steps: gas phase reactions of precursors in the deposition chamber (A), adsorption of reactive molecules at the surface (B), surface diffusion of adsorbed species (C) and finally the surface reaction leading to bulk deposition (D). While each of these steps can be present in a CVD process, it has been shown that surface diffusion (step C) is negligible for tungsten deposition [7]. Furthermore, in the remainder of this section we concentrate on feature scale aspects, assuming that step A has already taken place.

Under the above assumptions, steps B + D determine the (local) deposition rate and thus the step coverage of the process. At low temperatures, the deposition rate is generally limited by the surface reaction rate. This condition is referred to as the 'reaction-limited' process regime. On the other hand, at high process temperatures the surface reactions can be so fast that the transport of precursors to the surface is the deposition rate-limiting step. This regime is generally referred to as 'diffusion-limited' (or equivalently 'transport-limited'). This latter regime is usually employed for deposition on planar wafers, since under these conditions the process temperature has only minor impact on the deposition rate, and also because the throughput is maximized. However, for wafers with high aspect ratio structures (such as deep trenches), rapid surface reactions lead to precursor depletion inside deep trenches and, therefore, to a poor step coverage. A simplified way to look at surface reactions is assuming first-order reactions only. In this case the surface reaction rate can be expressed by the sticking probability η for particle–surface collision. A large sticking probability ($\eta = 1$) means that precursor molecules stick to the surface after the first collision. If, on the other hand, η is very small, it takes an average of $1/\eta$ collisions before precursor molecules stick to the surface. Since particles can only reach the bottom of a deep trench after *many* collisions with the sidewalls, it is evident that a good step coverage is only achieved if η is very small. This is equivalent to the extreme reaction-limited process regime.

In a gas the mean free path length λ is given by $\lambda = kT/(\sqrt{2}\sigma p)$, with k being the Boltzmann constant, T the gas temperature, σ the collision cross-section of the molecules and p the total pressure. Inside a deep trench, on the other hand, the mean path length between collisions is approximated well by the trench diameter, provided the latter is smaller than λ. In this so-called 'Knudsen regime' the step coverage of a process has been calculated analytically [8]:

$$\frac{t_B}{t_S} = \frac{1}{\cosh\phi + \frac{\phi W}{2L}\sinh\phi} \quad \text{with} \quad \phi = \frac{L}{W}\sqrt{\frac{3\eta}{2}} \tag{1}$$

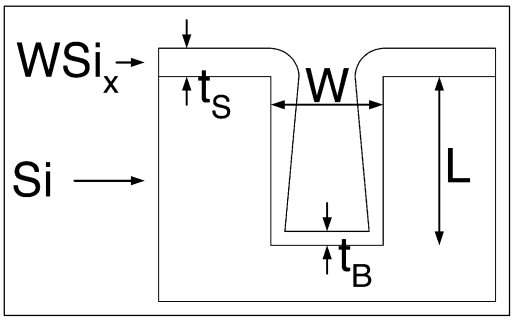

Fig. 1. Schematic of a layer deposited into a trench and definition of the variables in Eq. (1).

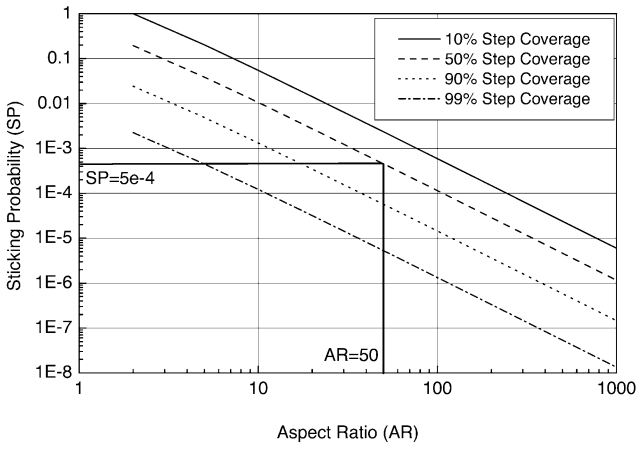

Fig. 2. Sticking probability η required to achieve a specific step coverage for a given aspect ratio as calculated using Eq. (1).

where η is the sticking coefficient and the other quantities are as explained in Fig. 1.

Eq. (1) indicates that for a given aspect ratio AR$=L/W$ the step coverage solely depends on the sticking coefficient η. To illustrate this behavior, Fig. 2 shows the η required to achieve a specific step coverage for a given aspect ratio. If, for instance, a trench with AR$=$ 50 is to be filled with 50% step coverage, the sticking coefficient should not exceed 5×10^{-4}. Note, however, that as the deposited film moves inwards, the AR continuously increases, resulting in a lower step coverage later on in the process [9].

3. Reaction chemistry

While the above arguments provide general insights into the properties of a suitable deep trench-CVD process, detailed studies are required to evaluate a specific chemistry. In this section we discuss some chemistries commonly used for planar WSi_x-CVD with focus on their applicability for high aspect ratio trench.

As follows from Sections 1 and 2, a WSi_x deep trench-CVD process has to simultaneously meet two requirements. On the one hand, the *total* sticking probability of the precursors has to be lower than approximately 5×10^{-4} in order to enable sufficient step coverage. On the other hand, the *individual* concentrations and sticking probabilities of the precursors need to be such that the composition of WSi_x is $x\approx2.3$ everywhere inside the trench. In the following text we will discuss several chemistries with respect to these requirements.

According to theoretical results [10], single-phase WSi_2 can be deposited using volatile organo-metallic tungsten precursors like $[H_2W(\eta^5\text{-}C_5H_5)_2]$ where η^5-C_5H_5 represents cyclo-pentadienyl. However, to our knowledge no experimental confirmation of this prediction has been published, let alone a production-worthy process. Mixed-phased layers are generally deposited using tungsten hexafluoride (WF_6) or tungsten carbonyl ($W(CO)_6$) [11–13]. In this paper we will only discuss WF_6 since it is the most commonly used tungsten precursor in the semiconductor industry. As silicon containing precursors, silane (SiH_4), disilane (Si_2H_6) and dichlorosilane (H_2SiCl_2, DCS) are all commonly used and are, therefore, considered in the following text.

For the CVD process using WF_6 and silane or disilane, it has been shown that the deposition rate crucially depends on the occurrence of a radical chain reaction in the gas phase [14]. With a process temperature above the so-called 'extinction temperature' (T_{ex}), the radical chain reaction rapidly saturates, and the concentration of reactive gas phase precursors does not depend on T. If, on the other hand, the reactor temperature is below T_{ex}, the chain reaction ceases and the deposition rate drops to 0 due to lack of reactive precursors [9]. It has been shown, however, that even in the case the *surface* temperature is well below T_{ex}, deposition can be achieved by heating the gas inlet (and thus initiating the radical chain reaction) [9]. Using this technique, CVD of WSi_x at temperatures as low as 313 K has already been demonstrated. It is important to note that under these conditions the step coverage is still determined by the surface temperature rather than by that of the inlet.

3.1. WF_6 and silane

Shimogaki et al. suggested a model for the gas phase reaction between WF_6 and silane that is similar to the disilane reaction discussed below [15,16]. According to this model the radical chain reaction leads to the following gas phase reaction:

$$\begin{aligned} &WF_6 + SiH_4 \rightarrow WF_5(SiH_3) + HF \\ &WF_{6-y} + (SiH_3)_y + SiH_4 \rightarrow WF_{5-y}(SiH_3)_{y+1} + HF \end{aligned} \qquad (2)$$

These reactions describe the successive replacement of fluorine by SiH_3 at thc WF_6-molecule. Assuming that deposition is mainly due to the resulting $WF_{6-z}(SiH_3)_z$ molecules [17] and that the above reactions have positive activation energy, this model correctly predicts an increasing Si content of the deposited layer for increasing temperature.

For the SiH_4/WF_6-system, Saito et al. have determined the total sticking probability η as a function of temperature [9]. The observed behavior is plotted in Fig. 3. For this chemistry, η is higher than the required 5×10^{-4} for all temperatures above room temperature. Additionally, the described chemical model predicts a composition close to $x=1$ for low temperatures. Both

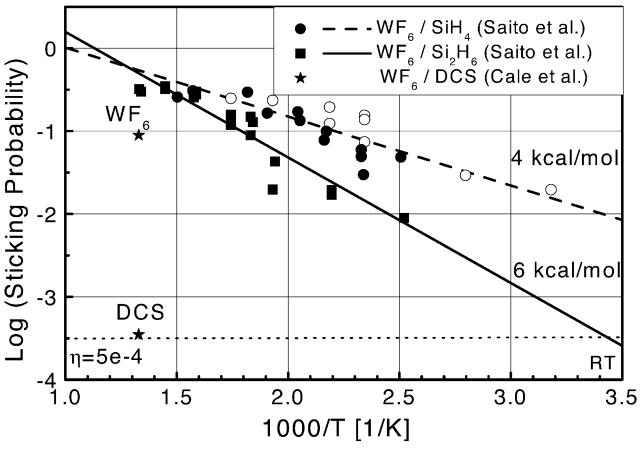

Fig. 3. Total sticking probabilities as a function of deposition temperature. Data is taken from [9] for the silane and the disilane processes and from [21] for the DCS process. The open and closed symbols represent depositions with and without preheating of precursors, respectively.

properties render this chemistry unsuitable for deep trench application, which will, therefore, not be considered further in this article.

3.2. WF_6 and disilane

While WF_6 decomposes at silicon surfaces [18], it has been shown experimentally that in the presence of sufficiently high concentrations of disilane (Si_2H_6) another reduction path dominates [14]. In this radical chain reaction, first proposed by Saito et al. [9], WF_6 is very efficiently reduced by an autocatalytic gas phase reaction. According to current understanding, the radical chain reaction is initiated immediately at the gas inlet by a thermal dissociation of WF_6 [14].

$$WF_6 \rightarrow \bullet WF_5 + \bullet F \tag{3}$$

Once this reaction has occurred, both resulting radicals can initiate a cascade of successive replacements of fluorine atoms by Si_2H_5-groups. In the case of the radical •F, this is

$$\bullet F + Si_2H_6 \rightarrow \bullet Si_2H_5 + HF$$

$$\bullet Si_2H_5 + WF_y(Si_2H_5)_{6-y} \rightarrow WF_{y-1}(Si_2H_5)_{7-y} + \bullet F \quad (y = 1 \ldots 6) \tag{4}$$

Similarly the $\bullet WF_5$, radical produced by the thermal dissociation Eq. (3) can also initiate a reduction chain reaction:

$$\bullet WF_5 + Si_2H_6 \rightarrow WF_5(Si_2H_5) + \bullet H \tag{5}$$

$$\bullet H + WF_6 \rightarrow \bullet WF_5 + HF$$

Again, this pair of reaction results in the reduction of WF_6, by a Si_2H_5-group while the reactive $\bullet WF_5$, radical is restored.

The reactions Eqs. (4) and (5) produce a significant amount of reactive $WF_y(Si_2H_5)_{6-y}$ precursors which can deposit at the surface. According to this model a higher Si/W ratio of the deposited layer is obtained by increasing the degree of reduction of WF_6. This can be achieved by heating either the substrate or the gas phase. Note, however, that in contrast to the WF_6/silane chemistry, here the film-forming species contains at least two silicon atoms per tungsten atom, even at low temperatures [14]. This favorable behavior is consistent with both, thermodynamic calculations [19] and experimental observations [9].

It has been shown by Kimbara that the minimum temperature (T_{ex}) to sustain the above radical chain reactions (and thus the deposition) depends on the surface-to-volume ratio (A/V) of the reactor [20]. Generally it is observed that increasing A/V also increases T_{ex}. According to Ref. [9] this dependence of the extinction temperature on reactor geometry is caused by a competing loss of reactive radicals to the reactor walls:

$$\bullet WF_5 + \bullet Si_2H_5 \rightarrow WF_5(Si_2H_5)$$

$$2\bullet H \rightarrow H_2$$

$$2\bullet F \rightarrow F_2 \tag{6}$$

$$\bullet H + \bullet F \rightarrow HF$$

$$\cdots$$

If the loss of radicals overcomes their production (Eq. (3)) the chain reaction ceases and the deposition rate drops to 0 due to lack of reactive precursors [9].

Though the above gas phase chemistry model provides a thorough understanding of Si_2H_6/WF_6-based CVD, it has to be noted that no surface chemistry model exists for this process. Nevertheless, the experimentally obtained sticking coefficients plotted in Fig. 3 show that even at room temperature acceptable step coverage can only be achieved for moderate aspect ratios smaller than 50:1. Because of this limitation we consider the Si_2H_6/WF_6 chemistry inappropriate for deep trench-CVD and will not discuss it further in this study. Note, however, that for medium aspect ratio trenches this process seems to be well suited, especially because of its favorable Si/W-ratio of the deposited layers

Table 1
Kinetic parameters for Eq. (7) as given by Cale et al.

Phase	k_j [mol/(cm^2 s mTorr$^{(\beta_j+\gamma_j)}$)]	E_j (kcal/mol)	β_j	γ_j	K (1/mTorr)
Si	1.3×10^{19}	90	2	0	0
WSi_2	3.6×10^{30}	120	1	1	1000
W_5Si_3	9.5×10^{4}	40	0.5	1	0

3.3. WF_6 and dichlorosilane

In contrast to the two systems described above, there exists no gas phase reaction model for CVD based on H_2SiCl_2 (DCS) and WF_6. For this chemistry it is apparently assumed that either there is no relevant gas phase reaction, or that the gas phase reactions do not vary noticeably in the process range explored so far. However, Cale et al. have developed a *surface* chemistry model which summarizes the present state of knowledge for this system [21]. It accounts for the deposition of the desired WSi_2(b) phase, but also for the deposition of Si(b) and a tungsten-rich, meta-stable W_5Si_3(b) bulk phase. This model, which its developers have implemented into their feature scale simulator *Evolve* [22], consists of the following three surface reactions:

$$H_2SiCl_2 \rightarrow Si(b) + 2HCl$$

$$WF_6 + 4H_2SiCl_2 \rightarrow WSi_2(b) + 8HCl + SiF_4 + SiF_2 \qquad (7)$$

$$5WF_6 + 11H_2SiCl_2 \rightarrow W_5Si_3(b) + 22HCl + 7SiF_4 + SiF_2$$

The deposition rate, R_j, of these reactions has been parameterized by:

$$R_j = k_j \exp\left(-\frac{E_j}{RT}\right)\left(\frac{p_D^{\beta_j} p_F^{\gamma_j}}{1+Kp_F}\right)$$
$$j = \mathrm{Si(b)},\ \mathrm{WSi_2(b)},\ \mathrm{W_5Si_3(b)}$$

where k_j, is a prefactor, E_j the activation energy, p_F the WF_6 partial pressure and p_D the DCS partial pressure. β_j and γ_j are the respective reaction orders of DCS and WF_6. The rather unfamiliar factor on the right-hand side has been introduced in Ref. [21] to account for the experimental observation of Schmitz et al. that the deposition is inhibited by the reaction product SiF_4 [7]. Note that no inhibition has been observed for HCl which is produced in large quantities by the above reactions. The kinetic parameters for Eq. (7) are summarized in Table 1 [23].

Because of the lack of literature data on the DCS/WF_6-chemistry at low temperatures it is quite difficult to decide whether this system is suitable for deep trench-CVD. Still, extrapolating the above model to low temperatures might already reveal some problems that can occur at low temperatures.

Even without quantitative analysis it is evident that the relative activation energies of the above model favor the deposition of the tungsten-rich W_5Si_3(b) phase at low temperatures. This trend is consistent with experimental data that will be shown in Section 4. Since, a Si/W ratio of 0.6 is unacceptable for deep trench-CVD for stability reasons (Section 1), it is apparent that this behavior is a major drawback of the DCS chemistry (especially compared to disilane). However, very high DCS and very low WF_6 partial pressures might suffice to counteract this effect.

A great advantage of the DCS/WF_6 chemistry as compared to silane and disilane is the much lower fluorine and chlorine bulk concentration, the low mechanical stress, and the better adhesion [4]. It has been observed that the F and Cl bulk concentrations increase with deposition temperature, a trend which is opposite to that in most other impurities [24]. However, both concentrations exhibit no measurable dependence of the individual flow rates.

A possible problem for a DCS/WF_6-based deep trench-CVD process is the experimental observation that the initial reduction of WF_6 is by the silicon–substrate rather than by DCS. This effect leads to a tungsten rich layer at the interface that is covered by other phases [18]. While these W-rich layers disappear at high deposition temperatures they might cause a problem at low temperatures.

Summarizing the DCS/WF_6-chemistry we can state that this system offers some advantages (low F/Si concentrations, low stress, good adhesion) but also includes some drawbacks (high W content at low T, W-rich interface). However, it is hard to decide about this chemistry since the model in Ref. [21] has only been calibrated to a narrow temperature range between 733 and 813 K and experimental data for low T are sparse. The only available measurement of the *individual* sticking coefficients in Fig. 3 indicates that especially the value for WF_6 is far too high at 753 K. This implies that still much lower temperatures are required to fill a high aspect ratio feature with uniform stoichiometry.

4. Experimental

To fill the gap in the experimental data base and to determine the individual sticking coefficients of DCS

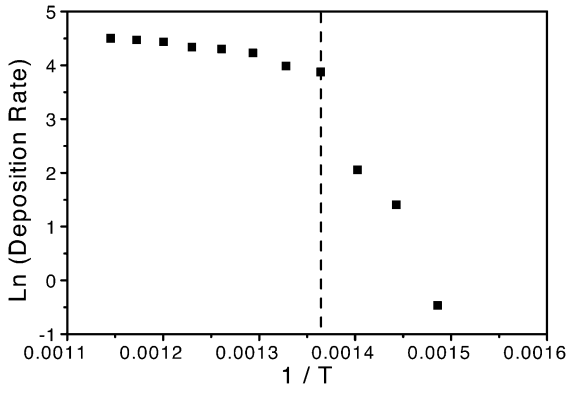

Fig. 4. Experimental deposition rate as a function of temperature for a DCS:WF_6 flow ratio of approximately 50:1 and a total chamber pressure of 1.2 Torr.

and WF_6 as a function of temperature we have performed the experiments described in the following. The experimental setup and the results are presented in this section. All experiments presented here have been performed in an 8-inch Applied Materials *Centura* single wafer tool using WF_6 and DCS as precursors and argon as carrier gas. In order to be consistent with earlier measurements [25] and with the above chemistry-model the wafer temperature was assumed to be 50 K lower than the measured chuck temperature.

Fig. 4 shows an Arrhenius plot of the measured deposition rate on blanket wafers for a DCS:WF_6 flow ratio of approximately 50:1 and a total chamber pressure of 1.2 Torr. The exponential decrease at low temperatures indicates that in this regime the deposition rate is limited by thermally activated reactions.

However, at temperatures above 750 K the deposition rate levels off to a maximum at 80 nm/min. In this regime, which is dependent on chamber design, total pressure, and the precursor flux, the deposition rate is limited by the transport of reactive species to the surface. The transition between the two regimes is indicated by a vertical line.

In order to determine the step coverage in the respective regimes deposition experiments on structured wafers have also been performed. Scanning electron microscope (SEM) images of the top of a deep trench are shown in Fig. 5. It is clearly visible that at 873 K only little deposition occurs inside the deep trench while at 693 K a smooth layer with good conformality is deposited.

While the above measurements yield the *total* sticking coefficient as a function of temperature (and thus the step coverage) they reveal nothing about the *individual* sticking probabilities (and thus the stoichiometry of the deposited layer). To access these we have performed additional experiments.

A common tool to measure bulk composition is Rutherford backscattering (RBS). But, since this technique is both tedious and expensive we also applied the much faster and cheaper method of measuring the thickness using SEM and the film resistivity using a four-point probe. Proof that this simple method is sufficient to determine bulk stoichiometry of WSi_x-films is shown in Fig. 6 where data from Refs. [18,26] as well as our own data are plotted. The composition of all data point marked as 'experiment' was determined by RBS measurements in this study. Once we calibrated this analysis with the obtained RBS results, we used thickness and resistivity as preferred method to determine

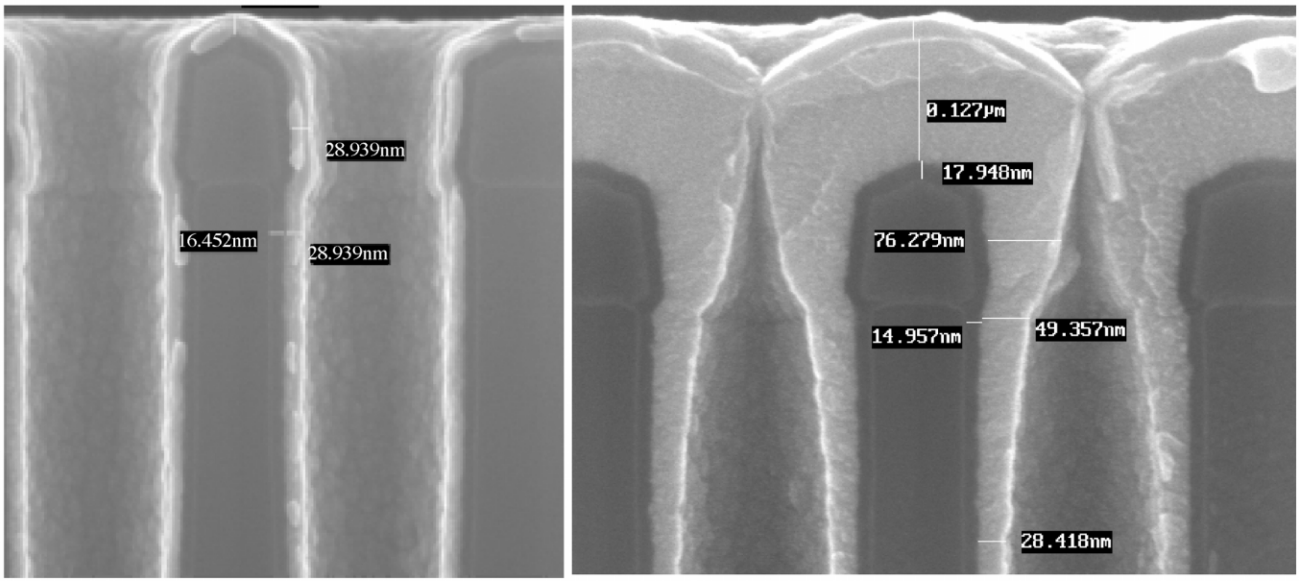

Fig. 5. SEM images of a WSi_x-layer deposited in DTs with an aspect ratio of 40:1. Layers were deposited at 693 K (left image) and at 873 K (right image).

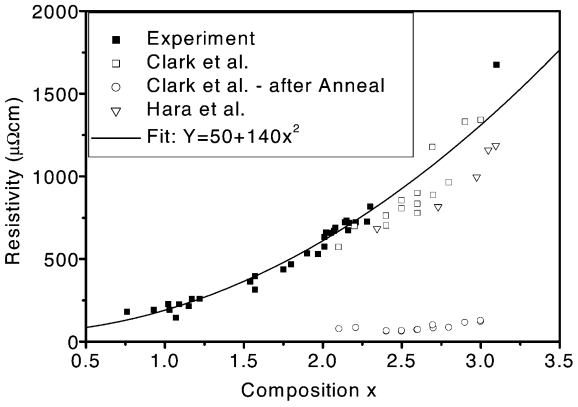

Fig. 6. Specific resistivity of tungsten silicide layers as a function of composition. Included in the graph are data from Clark [26], from Hara et al. [18] as well as new data (Experiment) and a quadratic fit to the data. Resistivity after an anneal shows only minor influence on composition.

composition. As it is apparent, the specific resistivity of the as-deposited film depends quadratically on stoichiometry. This relation can thus be used to determine the Si/W ratio of as-deposited filmy from measurements of the specific resistivity. Note that this strong dependence is lost after thermal annealing where a resistivity of approximately 65 $\mu\Omega$ cm is achieved as reported also by others [27].

Using this technique, the bulk composition is measured as a function of deposition temperature. The obtained stoichiometries are presented in Fig. 7. According to our data, silicon-rich WSi_x is deposited at a temperature above 820 K while the silicon content steadily decreases to 1.0 at 723 K.

From the measured planar deposition rate and stoichiometry the *individual* sticking probabilities of the precursors can be obtained from the kinetic gas theory as follows: given the surface temperature T_s and the partial pressure of a molecule p_j its deposition rate R_j is determined by the surface flux J_j, and the sticking probability η_j

$$R_j = \eta_j J_j \frac{M_d}{\rho_d} = \eta_j \frac{p_j}{\sqrt{2\pi M_j R T_s}} \frac{M_d}{\rho_d} \quad (8)$$

where M_j and M_d represent the precursor and bulk molar masses, and ρ_d the bulk density. Values for the species considered in this paper are summarized in Table 2. The sticking coefficients for DCS and WF_6 obtained from the above data and also from data by Raupp et al. [25] are shown in Fig. 8.

Table 2
Molar masses and bulk densities of species involved in the WF_6 reduction by DCS [21]

	Si	WSi_2	W_5Si_3	DCS	WF_6
M_j (g/mol)				100	298
M_k (g/mol)	28	240	1004		
ρ_k (g/m^3)	2.2×10^6	9.3×10^6	14.55×10^6		

5. Simulation

For additional insight into CVD using WF_6 and DCS, we have performed extensive simulations based on the surface reaction model by Cale et al. [21]. The purpose of these studies is to identify process conditions under which both a good step coverage and a Si/W ratio of $\approx$2.3 are achieved along the total length of the deep trench.

Once calibrated, simulations are performed within minutes and give easy access to the step coverage and the stoichiometry inside the deep trench which is hard to measure experimentally. However, it is important to remember that for deep trench-CVD the chemistry model in Ref. [21] needs to be pushed far beyond its validated

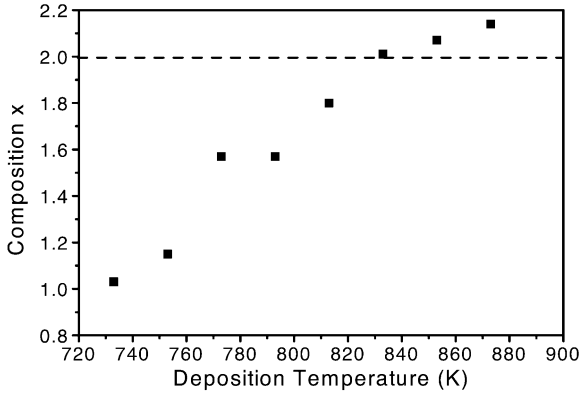

Fig. 7. Measured bulk composition as a function of deposition temperature for a DCS:WF_6 flow ratio of approximately 50:1 and a total chamber pressure of 1.2 Torr.

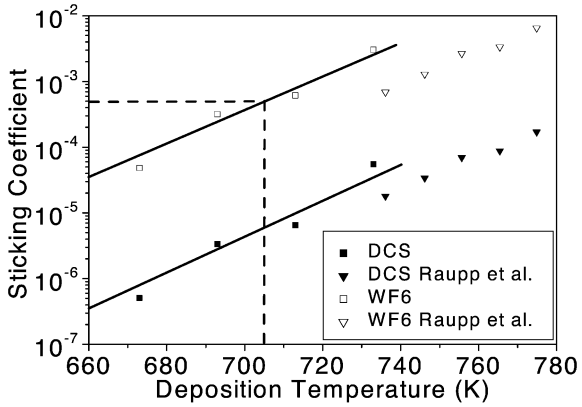

Fig. 8. Sticking coefficients (η) of DCS and WF_6 as a function of temperature, as determined from the deposition rate. Also shown are the η calculated from data by Raupp et al. [25].

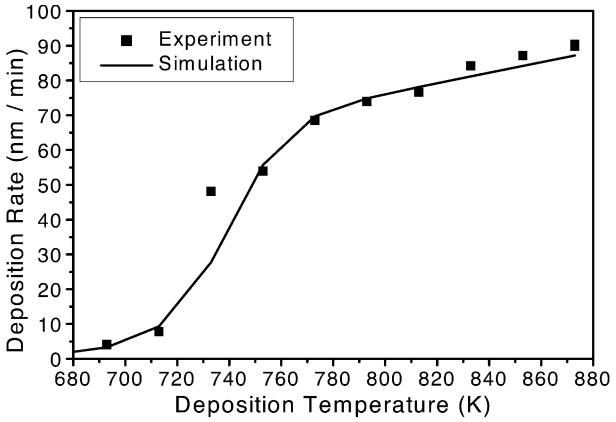

Fig. 9. Measured and simulated deposition rate as a function of temperature for a DCS:WF_6 flow ratio of approximately 50:1 and a total chamber pressure of 1.2 Torr.

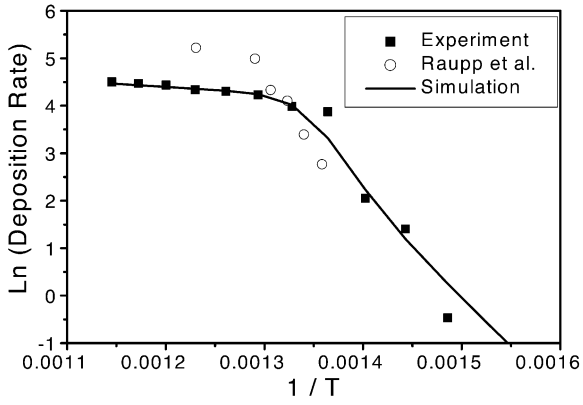

Fig. 10. Arrhenius plot of the reaction rate of Fig. 9.

parameter space. Thus, the simulation results presented below should be considered with appropriate care.

Two different types of simulations have been performed in this study, namely the deposition on planar wafers and into deep trenches. For the simulation of planar deposition we assume that the surface of the wafer is connected to a reservoir of constant precursor partial pressures via a diffusion channel. This channel is required to account, for the transport limitation at elevated temperatures. For given process (reservoir) conditions detailed balance requires that the molar loss at the reactive surface (given by Eq. (7), [21]) is equal to the diffusion flux through the transport channel which is governed by Fick's first law:

$$J_j = -D_j \nabla n_j \qquad (9)$$

$$D_j = v_{\text{therm}} \lambda$$

where ∇n_j is the concentration gradient of the molecules, $v_{\text{therm}} = \sqrt{2kT/m}$ the average thermal velocity and λ the mean free path of the precursors as described in Section 2. Given the length of the depletion zone the precursor partial pressures at the wafer surface are varied until the loss through reactions equals the respective flux towards the surface. Here the collision cross-section can be estimated whereas the depletion length has to be fitted to experimental data.

Fig. 9 compares the simulated deposition rate to the experimental data shown in Fig. 4. It can be seen that the overall agreement with experiment is rather satisfactory. For the reaction-limited regime, which is important for deep trench-CVD, an Arrhenius plot of the deposition rate is shown in Fig. 10. Taking into account an offset of 50 K between measured chuck temperature and wafer temperature, this regime is also described reasonably well by the reaction rates given in Ref. [21]. But while the planar deposition rate is simulated quite well, Fig. 11 shows that the simulated Si/W ratio as a function of temperature differs significantly from the experimental data. This indicates that the chemistry model in Ref. [21] is less accurate under the rather extreme process conditions studied here.

Besides modelling planar deposition rates and Si/W ratio we have developed a simulator (*Knudsim*) which calculates the *local* deposition rate and stoichiometry inside a circular deep trench. Here, the main problem (and the key to its solution) lies in the extreme aspect, ratio of 50:1 or more. While simulators like *Evolve* give reliable results for deposition into comparably shallow features [21] they are generally unsuitable for structures with very high aspect ratios. This is due to the fact that an accurate calculation of the transport inside a deep trench requires either, massive CPU power, massive memory, or both. *Evolve*, for instance, solves the transport problem using the view-factor method which involves very large matrices for large aspect ratios. To avoid these problems we have exploited the quasi-1D

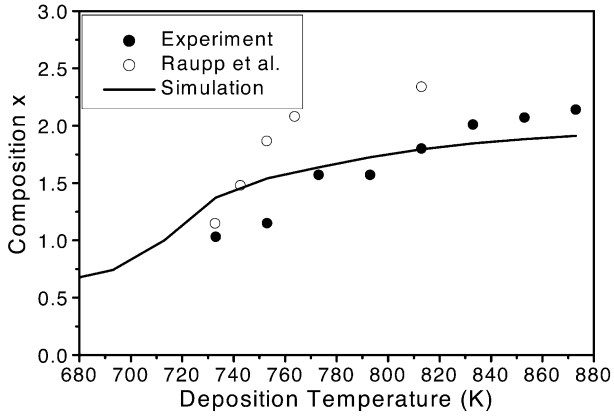

Fig. 11. Measured and simulated Si/W ratio x as a function of deposition temperature for a DCS:WF_6 flow ratio of approximately 50:1 and a total chamber pressure of 1.2 Torr.

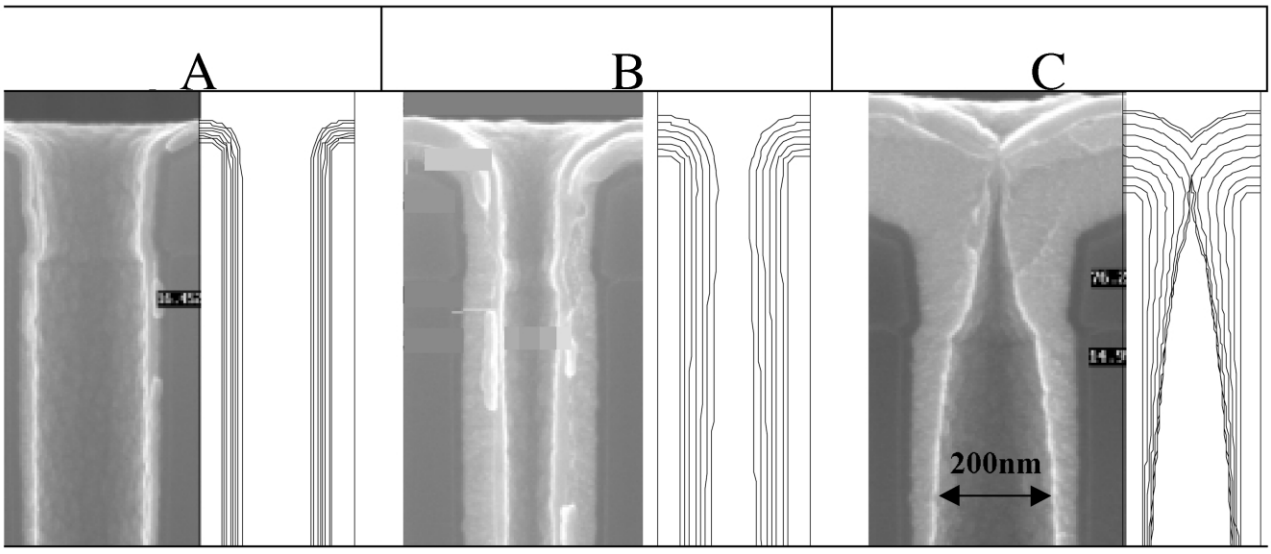

Fig. 12. Experimental and simulated structures for three different temperatures. 'A' represents reaction-limited CVD at 693 K; 'B' the transition of reaction to diffusion-limited deposition at 713 K; and 'C' the deposition in the diffusion-limited regime at 783 K.

geometry of deep trenches and assume that inside the deep trench the concentration is independent on radius. This is a reasonable approach since under typical CVD conditions today's trench diameters are orders of magnitude smaller than the mean free path in the gas.

Assuming this kind of 1D transport the diffusion inside the deep trench is also governed by Fick's first law (Eq. (9)) but with the (Knudsen-)diffusion constant now given by:

$$D_j \approx v_{j,\mathrm{therm}} d \tag{10}$$

where d is the diameter of the deep trench. As in the above case of planar deposition detailed balance requires that the molar loss due to surface reactions is equal to the diffusion flux. But while the surface reactions occur *after* the transport through the depletion zone, inside the deep trench transport and deposition occur simultaneously.

In order to obtain the precursor concentrations θ_j of WF_6 and DCS we divide the deep trench into segments of length l and iteratively solve the equation for the steady state of $\theta_{j,i}$ at each discrete position *i.*

$$0 \equiv \frac{\partial \theta}{\partial t} = -\frac{D_j}{l}(2\theta_{j,i} - \theta_{j,i+1} - \theta_{j,i-1}) + \sum_{k=1}^{3} R_k(\theta_{1,2}) \tag{11}$$

where the reaction rates R_j are those from Section 3.3. To solve Eq. (11) we use successive overrelaxation until convergence is achieved. Given the precursor concentrations $\theta_{j,i}$ the *local* deposition rate (step coverage) and stoichiometry (x) are readily obtained from the reaction rates 7.

In order to study the impact of increasing aspect ratio during the process we have coupled the above described *Knudsim* simulator to our custom feature scale simulator *Topsi.* In each timestep the *local* diameter d_i of the trench is obtained from the simulated front (*Topsi*). Using d_i, the normal velocity for each front segment is calculated using *Knudsim.* The front is then propagated (*Topsi*) using the levelset algorithm [28] before the next timestep is computed.

Fig. 12 shows a comparison of the thus obtained structures with SEM images for three different temperatures and 'standard' precursor concentrations. 'A' shows a reaction limited deposition at 693 K, 'B' a deposition at 713 K in the transition regime between reaction and diffusion limited and 'C' a diffusion limited deposition at 783 K. As can be seen the step coverages and overall shapes of the evolved structures agree very well for all temperatures.

In order to identify a process with both good step coverage and an uniform stoichiometry $Si/W \approx 2.3$ we have performed an optimization of the free parameters p_{DCS}, $p_{\mathrm{WF_6}}$ and T with respect to these properties. Our simulations suggest such a regime below 650 K, a DCS partial pressure of 2–10 Torr and a WF_6 partial pressure of several mTorr.

6. Discussion

Already the general discussion of growth kinetics yielded that a deep trench-CVD process needs to be reaction limited in order to have a good step coverage inside high aspect ratio structures. Assuming an aspect ratio of 50:1 and a targeted 50% step coverage relation 1 (or Fig. 2) indicates that the total sticking coefficient η has to be lower than 5×10^{-4}. For the chemistry

discussed here this in turn implies a deposition temperature well below 700 K as shown in Fig. 8.

While very low process temperatures might solve the problem of insufficient step coverage it has been shown experimentally that WF_6/DCS-based CVD produces tungsten-rich layers which are unsuitable for deep trench applications. However, the simulations presented in Section 5 suggest that the higher deposition rate of W can be countered by (drastically) increasing the DCS partial pressure while decreasing the WF_6 concentration. While the proposed process conditions are far beyond the calibrated parameter space of the chemistry model in Ref. [21] the prospect of metallic deep trench plugs and vias has already triggered respective experiments which are currently performed.

Cale et al. have demonstrated that CVD using WF_6 and DCS is inherently transient in nature [21]. This means that the composition of the film changes during the deposition in a trench due to the change in aspect ratio. Compositional changes during the process are observed already with an aspect ratio of 5:1. When the opening of a structure shrinks the Knudsen diffusion of the reactants into the trench slows down and the deposition rate decreases. While this effect is correctly modelled by our combined *Knudsim+Topsi* simulator all above simulation results (with file exception of Fig. 12) were obtained without accounting for local and transient trench diameters. Thus, the results presented here only represent the initial timestep in the process. If, however, the currently performed experiments turn out promising, further refinements of the parameters can be achieved by fully transient simulations.

For the extremely low sticking probabilities η required for deep trench-CVD the deposition rate necessarily is very low. For a first-order reaction and a given precursor pressure the deposition rate can be calculated using Eq. (8). For instance, deposition at partial pressure of 1 Torr and a sticking coefficient of 5×10^{-6} does not exceed 10 nm/min. For economic reason a production worthy deep trench-CVD process, therefore, needs to be either performed in a batch reactor or in a single wafer tool at higher pressures.

7. Conclusion

Using experiments and simulations we have identified the reduction of WF_6 by DCS as a promising candidate for CVD of WSi_2-layers into deep trenches with aspect ratios of $\geqslant$50:1. The simulations presented in this paper are based on a literature surface chemistry model and yield realistic step coverages over a wide range of temperature. Justified by these results we propose a CVD process with both good step coverage and suitable stoichiometry inside the deep trench. While conclusive experimental confirmation is still missing our simulations suggest that stoichiometric films with a step coverage of more than 50% can be deposited below 700 K if the DCS partial pressure is 2–3 orders of magnitude higher than the WF_6 pressure.

Acknowledgments

The authors would like to thank Stefan Jakschik for his great support.

References

[1] S. Wolf, R.N. Tauber, Silicon Processing for the VLSI Era, vol. 1, Lattice Press, Sunset Beach, 1988, p. 384.
[2] N. Thomas, P. Suryanarayana, E. Blanquet, C. Vahlas, R. Madar, C. Bernard, J. Electrochem. Soc. 140 (2) (1993) 475.
[3] K.C. Saraswat, D.L. Brors, J.A. Fair, K.A. Monnig, R. Beyers, IEEE Trans. Electron. Dev. ED-30 (1983) 1497.
[4] S.G. Telford, M. Eizenberg, M. Chang, A.K. Sinha, T.R. Gow, J. Electrochem. Soc. 140 (12) (1993) 3689.
[5] J.R. Chen, Y.K. Fang, S.L. Hsu, Vacuum 37 (3/4) (1987) 357.
[6] M. Katiyar, G.S. Samal, R.K. Gupta, Deepak, P.K. Sahoo, V.N. Kulkarni, O. Adetutu, Mater. Res. Soc. Symp. Proc., Materials Research Society, 2001, p. K571.
[7] J.E.J. Schmitz, W.L.N.v.d. Sluys, A.H. Montree, in: G.C. Smith (Ed.), Tungsten and Other Advanced Metals for VLSI/ULSI Applications V, Materials Research Society, 1990, p. 117.
[8] Y. Shimogaki, T. Saito, F. Tadokoro, H. Komiyama, J. de Phys. IV Colloq. C2 suppl. au J. de Phys. II 1 (1991) 95.
[9] T. Saito, Y. Shimogaki, Y. Egashira, H. Komiyama, K. Sugawara, K. Takahiro, S. Nagata, S. Yamaguchi, Electron. Commun. Jpn., Part 2 78 (10) (1995) 73.
[10] F.A. Kuznetsov, V.A. Titov, A.N. Golubenko, A.A. Titov, Proceedings of SPIE, vol. 1783, The International Society for Optical Engineering, Warsaw, 1992, p. 541.
[11] K. Lai, H. Lamb, Thin Solid Films 370 (2000) 114.
[12] L.H. Kaplan, F.M. D'Heurle, J. Electrochem. Soc. 117 (1970) 693.
[13] F. Hamelmann, S. Petri, A. Klipp, G. Haindl, J. Hartwich, L. Dreeskornfeld, U. Kleineberg, P. Jutzi, U. Heinzmann, Thin Solid Films 338 (1999) 70.
[14] Y. Egashira, H. Aita, T. Saito, Y. Shimogaki, H. Komiyama, K. Sugawara, Electron. Commun. Jpn. Part 2 79 (1) (1996) 83.
[15] Y. Shimogaki, T. Saito, R. Ikawa, Y. Egashira, K. Sugawara, H. Komiyama, 11th International VLSI Multilevel Conference (VMIC), 1994, p. 496.
[16] Y.K. Chae, Y. Egashira, Y. Shimogaki, K. Sugawara, H. Komiyama, J. Electrochem. Soc. 146 (1999) 1780.
[17] Y.K. Chae, Y. Egashira, Y. Shimogaki, K. Sugawara, H. Komiyama, Thin Solid Films 320 (1998) 151.
[18] T. Hara, T. Miyamoto, H. Hagiwara, E.I. Bromley, W.R. Harshbarger, J. Electrochem. Soc. 137 (9) (1990) 2955.
[19] E.J. Rode, W.R. Harshbarger, J. Vac. Sci. Technol. B 8 (1) (1990) 91.
[20] K. Kimbara (Ed.), Gaseous Combustion Theory, Shokabo Press, 1985, p. 120.
[21] T.S. Cale, J.H. Park, G.B. Raupp, M.K. Jain, B.R. Rogers (Eds.), Advanced Metallization for ULSI Applications, Materials Research Society, Murray Hill, NJ, USA and Tokyo, Japan, 1992, p. 93.
[22] T.S. Cale, EVOLVE, developed at Arizona State University and Motorola Inc.

[23] T.S. Cale, T.H. Gandy, M.K. Jain, G.B. Raupp, M. Govil, A. Hasper (Eds.), Advanced Metallization for ULSI Applications, Materials Research Society, Murray Hill, 1992, p. 101.
[24] T.H.T. Wu, R.S. Rosler, B.C. Lamartine, R.B. Gregory, H.G. Tompkins, J. Vac. Sci. Technol. B 6 (6) (1988) 1707.
[25] G.B. Raupp, T.S. Cale, M.K. Jain, B. Rogers, D. Srinivas, Thin Solid Films 193/194 (1990) 234.
[26] T.E. Clark, J. Vac. Sci. Technol. B 6 (6) (1988) 1678.
[27] H. Yoon, C. Chen, A. Singhal, D. Lopes, G. Miner, S. Hong, Electrochemical Society Proceedings, vol. 10, 1999, p. 249.
[28] J.A. Sethian, Cambridge Monographs on Applied and Computational Mathematics, ISBN 0-521-64204-3.